Applications and Applied Mathematics: An International Journal (AAM)

Volume 12 | Issue 2 Article 21

12-2017

Heat and Mass Transfer Effects of Peristaltic Transport of a Nano Fluid in Peripheral layer

K. M. Prasad
GITAM University - Hyderabad Campus

N. Subadra
Geethanjali College of Engg. & Tech

M, A. S. Srinivas
JNTUH, Kukatpally

Available at
http://pvamu.edu/aam
Appl. Appl. Math.
ISSN: 1932-9466

Applications and Applied Mathematics:
An International Journal
(AAM)

Vol. 12, Issue 2 (December 2017), pp. 968 - 987

Heat and Mass Transfer Effects of Peristaltic Transport of a Nano Fluid in Peripheral layer

[1]K. Maruthi Prasad, [2*]N. Subadra and [3]M. A. S. Srinivas

[1]Department of Engineering Mathematics
School of Technology
GITAM University - Hyderabad Campus
Hyderabad Telangana India-502329
Email: kaipa_maruthi@yahoo.com

[*2]Department of Mathematics
Geethanjali College of Engg. & Tech
Cheeryal (V) , Keesara (M), Medchal Dist.
Telangana India-501301
Email: nemani.subhadra@gmail.com

[3]Department of Mathematics
JNTUH, Kukatpally
Hyderabad Telangana India-500085
Email: massrinivas@gmail.com

[*]Corresponding editor

Received: August 11, 2016; Accepted: October 11, 2017

Abstract

This paper deals with a theoretical investigation of heat and mass transfer effects of peristaltic transport of a nanofluid in peripheral layer. By using appropriate methods, the velocity in the core region as well as in the peripheral region, pressure drop, time averaged flux, frictional force, temperature profile, nanoparticle phenomenon, heat transfer coefficient and mass transfer coefficient of the fluid are investigated, using lubrication theory. Effects of different physical parameters like viscosity ratio, mean radius of the central layer, Brownian motion parameter, thermophoresis parameter, local temperature Grashof number as well as local nanoparticle Grashof number on pressure rise characteristics, frictional force, heat transfer coefficient, mass transfer coefficient, velocity profiles and streamline patterns of the fluid are studied. The computational results are presented in graphical form.

Keywords: Peristalsis; Nano fluid; Homotopy perturbation method; Peripheral Layer; Heat transfer coefficient; Mass transfer coefficient

MSC 2010 No.: 92C10, 76Z05

1. Introduction

Peristaltic transport is an important mechanism used to describe a progressive wave of contraction along the tube whose cross sectional area consequently varies. Peristalsis is an inherent property of many tubular organs of the human body. The peristaltic transport is also exploited for industrial applications like transport of corrosive and noxious fluids, blood pumps in heart lung machine, sanitary fluid transport. In view of its importance, the study of peristaltic transport of Newtonian and non-Newtonian fluids under different conditions have been investigated by several authors [Latham (1966), Fung and Yih (1968), Shapiro et al. (1969), Devi & Devanathan (1975), Meijing et al. (1993), Prasad & Radhakrishnamacharya (2009), Pincombe et al. (1999), Prasad et. al. (2015), Santhosh et al. (2015)].

It is realized that the materials of nanometer dimensions have shown remarkable physical and chemical properties which paved the way for the immense contribution of Nanotechnology in the industry. Ethylene glycol, oil and water are the general base fluids used for the nanofluid phenomenon. The wider applications of nano fluids in heat transfer are Microelectronics, fuel cells, pharmaceutical processes, hybrid-powered engines, domestic refrigerator, chiller, nuclear reactor coolant, grinding and space technology, etc. They explore increased thermal conductivity, counterbalancing the convective heat transfer coefficient to the base fluid. Several researchers' attention has been drawn by the wide-ranging thermal properties of nano fluids for new production of heat transfer fluids in automotive cooling significations, heat exchangers, and implants. Extensive literature is available on the study of nanofluid and its applications.

Choi (1995) was the pioneer of study of nano fluid technology. Peristaltic flow of nano fluid in a non-uniform tube was studied by Akbar (2012). Mathematical model for the peristaltic flow of nano fluid through eccentric tubes comprising porous medium was investigated by Nadeem et al. (2014). Nadeem et al. (2014) studied effects of heat and mass transfer on peristaltic flow of a nano fluid between eccentric cylinders. Study of peristaltic transport of nanoparticles of micropolar fluid with heat and mass transfer effect in an inclined tube was investigated by Prasad et al. (2015). Maruthi Prasad et al. (2015) also studied Peristaltic transport of a nano fluid in an inclined tube.

It is well known that in many physiological flows, the nature of the fluid at the core region of the tube is different compared to that near the wall. So several researches have done work on the effect of peripheral layer on peristaltic flow of fluids with particular reference to physiological systems. Effects of peripheral layer on peristaltic transport of a bio-fluid was studied by Shukla et al. (1980). Srivastava and Srivastava (1982) investigated peristaltic transport of a two-layered model of physiological fluid. Brasseur et al. (1987) studied the influence of a peripheral layer of different viscosity on peristaltic pumping with Newtonian fluids. Rao and Usha (1995) studied

peristaltic transport of two immiscible viscous fluids in a circular tube. Prasad & Radhakrishnamacharya (2009) investigated the effect of peripheral layer on peristaltic transport of a couple-stress fluid. Effect of peripheral layer on peristaltic transport of a micropolar fluid was studied by Prasad and Radhakrishnamacharya (2009). However, the study of effect of peripheral layer on peristaltic transport of a nano fluid was not studied.

Motivated by these studies, the study of effect of peripheral layer on peristaltic transport of a nano fluid, under the assumption of long wavelength and low Reynolds number has been done. To solve the resulting equations of the temperature profile and nanoparticle phenomena, Homotopy perturbation method has been used. The analytical solutions of velocity, pressure drop, frictional force and effect of heat and mass transfer are obtained. The effects of various parameters on these flow variables are investigated and graphically displayed.

2. Mathematical Formulation

Consider the peristaltic transport of a nano fluid which is surrounded by Newtonian fluid in an axisymmetric tube of radius a, with core radius a_1. Choosing the polar coordinate system (R, θ, Z), the wall deformation due to propagation of an infinite train of peristaltic waves is given by

$$R = H(Z,t) = a + b \sin \frac{2\pi}{\lambda}(Z - ct), \tag{1}$$

where, b is the amplitude, λ is the wave length, c is the speed of the wave.

Following Prasad et al. (2009) the geometry of the interface between the peripheral layer and core region is

$$R = H_1(Z,t) = a_1 + b_1 \sin \frac{2\pi}{\lambda}(Z - ct), \tag{2}$$

where, a_1 is the mean radius and b_1 is the amplitude of the central layer.

We use the transformation

$$\bar{z} = \bar{Z} - c\bar{t}, \;\; \bar{r} = \bar{R}, \; \theta = \theta, \; \bar{w} = \bar{W} - c, \quad \bar{u} = \bar{U}. \tag{3}$$

From a stationary to moving frame of reference, the equations of motion in two regions are given as follows:

(a) Peripheral region $(\boldsymbol{H_1(z) \le r \le H(z)})$:

$$\frac{\partial \bar{p}}{\partial \bar{z}} = \mu_p \nabla^2 \overline{w_1}, \tag{4}$$

$$\frac{\partial \bar{p}}{\partial \bar{r}} = 0, \tag{5}$$

where, $\nabla^2 = \frac{\partial^2}{\partial r^2} + \frac{1}{r}\frac{\partial}{\partial r} + \frac{\partial^2}{\partial z^2}$, $\overline{w_1}$ is the component velocity in z-direction, $\bar{p}$ is the pressure and μ_p is the constant viscosity of Newtonian fluid in the peripheral region.

(b) Core Region($0 \le r \le H_1(z)$):

The law of conservation of mass, momentum, energy and nanoparticle concentration for an incompressible nanofluid are described by Nadeem et al. (2014) as

$$\frac{1}{\bar{r}}\frac{\partial(\bar{r}\bar{u})}{\partial \bar{r}} + \frac{\partial \bar{w}}{\partial \bar{z}} = 0, \tag{6}$$

$$\rho\left[\bar{u}\frac{\partial \bar{u}}{\partial \bar{r}} + \bar{w}\frac{\partial \bar{u}}{\partial \bar{z}}\right] = -\frac{\partial \bar{P}}{\partial \bar{r}} + \mu_c\left[\frac{\partial^2 \bar{u}}{\partial \bar{r}^2} + \frac{1}{\bar{r}}\frac{\partial \bar{u}}{\partial \bar{r}} + \frac{\partial^2 \bar{u}}{\partial \bar{z}^2} - \frac{\bar{u}}{\bar{r}^2}\right], \tag{7}$$

$$\rho\left[\bar{u}\frac{\partial \bar{w}}{\partial \bar{r}} + \bar{w}\frac{\partial \bar{w}}{\partial \bar{z}}\right] = -\frac{\partial \bar{P}}{\partial \bar{z}} + \mu_c\left[\frac{\partial^2 \bar{w}}{\partial \bar{r}^2} + \frac{1}{\bar{r}}\frac{\partial \bar{w}}{\partial \bar{r}} + \frac{\partial^2 \bar{w}}{\partial \bar{z}^2}\right] + \rho g\beta(\bar{T} - \overline{T_o}) + \rho g\beta(\bar{C} - \overline{C_o}), \tag{8}$$

$$\left[\bar{u}\frac{\partial \bar{T}}{\partial \bar{r}} + \bar{w}\frac{\partial \bar{T}}{\partial \bar{z}}\right] = \beta\left[\frac{\partial^2 \bar{T}}{\partial \bar{r}^2} + \frac{1}{\bar{r}}\frac{\partial \bar{T}}{\partial \bar{r}} + \frac{\partial^2 \bar{T}}{\partial \bar{z}^2}\right] + \tau\left\{D_B\left[\frac{\partial \bar{C}}{\partial \bar{r}}\frac{\partial \bar{T}}{\partial \bar{r}} + \frac{\partial \bar{C}}{\partial \bar{z}}\frac{\partial \bar{T}}{\partial \bar{z}}\right] + \frac{D_{\bar{T}}}{\overline{T_o}}\left[\left(\frac{\partial \bar{T}}{\partial \bar{r}}\right)^2 + \left(\frac{\partial \bar{T}}{\partial \bar{z}}\right)^2\right]\right\}, \tag{9}$$

$$\left[\bar{u}\frac{\partial \bar{C}}{\partial \bar{r}} + \bar{w}\frac{\partial C}{\partial \bar{z}}\right] = D_B\left[\frac{\partial^2 \bar{C}}{\partial \bar{r}^2} + \frac{1}{\bar{r}}\frac{\partial \bar{C}}{\partial \bar{r}} + \frac{\partial^2 \bar{C}}{\partial \bar{z}^2}\right] + \frac{D_{\bar{T}}}{\overline{T_o}}\left[\frac{\partial^2 \bar{T}}{\partial \bar{r}^2} + \frac{1}{\bar{r}}\frac{\partial \bar{T}}{\partial \bar{r}} + \frac{\partial^2 \bar{T}}{\partial \bar{z}^2}\right], \tag{10}$$

where $\bar{u}$ and $\overline{w}$ represent the radial and axial velocity components in the wave frame, μ_c is the viscosity of the nano fluid in the core region, $\frac{d}{dt}$ represents the material time derivative, $\bar{p}$ is the pressure, $\bar{C}$ is the nanoparticle phenomena, $\tau = \frac{(\rho C)_P}{(\rho C)_f}$ is the ratio between the effective heat capacity of the nanoparticle material and heat capacity of the fluid, D_B is the Brownian diffusion coefficient and $D_{\bar{T}}$ is the thermophoretic diffusion coefficient. The ambient values of $\bar{T} and\ \bar{C}$ as $\bar{r}$ tend to $\bar{h}$ are denoted by $\overline{T_o}$and$\overline{C_o}$.

We introduce the following non-dimensional quantities

$$r = \frac{\bar{r}}{a}, \quad z = \frac{\bar{z}}{\lambda}, \quad w = \frac{\overline{w}}{c}, \quad u = \frac{\lambda \bar{u}}{ac}, \overline{w_1} = \frac{w_1}{c},$$

$$p = \frac{a^2\bar{p}}{c\lambda\mu_c}, \theta_t = \frac{\bar{T} - \overline{T_o}}{\overline{T_o}}, t = \frac{c\bar{t}}{\lambda}, \delta = \frac{a}{\lambda}, R_e = \frac{2\rho ca}{\mu_c}, \sigma = \frac{\bar{C} - \overline{C_o}}{\overline{C_o}},$$

$$\beta = \frac{K}{(\rho C)_f}, \quad N_b = \frac{(\rho C)_P D_{\bar{B}}\overline{C_o}}{(\rho C)_f}, \quad N_t = \frac{(\rho C)_P D_{\bar{T}}\overline{T_o}}{(\rho C)_f \beta},$$

$$N_t = \frac{(\rho C)_P D_{\bar{T}}\overline{T_o}}{(\rho C)_f \beta}, \quad G_r = \frac{g\beta a^3 \overline{T_o}}{\varphi^2}, \quad B_r = \frac{g\beta a^3 \overline{C_o}}{\varphi^2}, \quad \varphi^2 = \frac{\mu_c}{\rho},$$

in which N_b, N_t, G_r and B_r are the Brownian motion parameter, the Thermophoresis parameter, local temperature Grashof number and local nanoparticle Grashof number.

Using the non-dimensional quantities and applying the long wavelength and low Reynolds number approximations, Equations (4) - (10) are converted to

$$\frac{\partial p}{\partial z} = \frac{1}{r}\frac{\partial}{\partial r}\left(\bar{\mu} r \frac{\partial}{\partial r}\right) w_1, \tag{11}$$

$$\frac{\partial P}{\partial r} = 0, \tag{12}$$

$$\frac{\partial u}{\partial r} + \frac{u}{r} + \frac{\partial w}{\partial z} = 0, \tag{13}$$

$$\frac{\partial P}{\partial z} = \frac{1}{r}\frac{\partial}{\partial r}\left(r \frac{\partial w}{\partial r}\right) + G_r \theta_t + B_r \sigma, \tag{14}$$

$$0 = \frac{1}{r}\frac{\partial}{\partial r}\left(r \frac{\partial \theta_t}{\partial r}\right) + N_b \frac{\partial \sigma}{\partial r}\frac{\partial \theta_t}{\partial r} + N_t \left(\frac{\partial \theta_t}{\partial r}\right)^2, \tag{15}$$

$$0 = \frac{1}{r}\frac{\partial}{\partial r}\left(r \frac{\partial \sigma}{\partial r}\right) + \frac{N_t}{N_b}\left(\frac{1}{r}\frac{\partial}{\partial r}\left(r \frac{\partial \theta_t}{\partial r}\right)\right), \tag{16}$$

where, $\bar{\mu} = \frac{\mu_p}{\mu_c}$ is the viscosity ratio.

The non-dimensional boundary conditions are

$$w_1 = 0 \text{ at } r = h = 1 + \varepsilon \sin 2\pi z, \tag{17}$$

$$\frac{\partial w}{\partial r} = 0,\ \frac{\partial \theta_t}{\partial r} = 0,\ \frac{\partial \sigma}{\partial r} = 0 \ at\ r = 0, \tag{18}$$

$$\theta_t = 0,\ \sigma = 0 \ \ at\ r = h_1(z) = \delta + \varepsilon_1 \sin 2\pi z, \tag{19}$$

$$w_1 = w\ at\ r = h_1(z), \tag{20}$$

$$\bar{\mu}\frac{\partial w_1}{\partial r} = \frac{\partial w}{\partial r} + \frac{r}{2}(G_r \theta_t + B_r \sigma)\ at\ r = h_1(z). \tag{21}$$

Following the analysis of Shukla et al. (1980) it is taken that $h_1 = \delta h$ and $\varepsilon_1 = \delta \varepsilon$

3. Solution of the Problem

Solving Equation (11), using the boundary condition (17), the expression for w_1 is

$$w_1 = \frac{r^2 - h^2}{4\bar{\mu}}\frac{dp}{dz} + \frac{c_1}{\bar{\mu}} \log\left(\frac{r}{h}\right). \tag{22}$$

By applying homotopy technique for Equations (15) and (16), the equations become

$$H(\zeta,\theta_t) = (1-\zeta)\left[L(\theta_t) - L\left(\theta_{t_{10}}\right)\right] + \zeta\left[L(\theta_t) + N_b\frac{\partial\sigma}{\partial r}\frac{\partial\theta_t}{\partial r} + N_t\left(\frac{\partial\theta_t}{\partial r}\right)^2\right], \tag{23}$$

$$H(\zeta,\sigma) = (1-\zeta)[L(\sigma) - L(\sigma_{10})] + \zeta\left[L(\sigma) + \frac{N_t}{N_b}\left(\frac{1}{r}\frac{\partial}{\partial r}\left(r\frac{\partial\theta_t}{\partial r}\right)\right)\right], \tag{24}$$

where $L = \frac{1}{r}\frac{\partial}{\partial r}\left(r\frac{\partial}{\partial r}\right)$ is taken as linear operator for convenience.

Consider

$$\theta_{10}(r,z) = \left(\frac{r^2-h^2}{4}\right), \quad \sigma_{10}(r,z) = -\left(\frac{r^2-h^2}{4}\right), \tag{25}$$

as initial guesses which satisfy the boundary conditions.

Define

$$\theta_t(r,z) = \theta_{t_0} + \zeta\theta_{t_1} + \zeta^2\theta_{t_2} + \cdots, \tag{26}$$

$$\sigma(r,z) = \sigma_0 + \zeta\sigma_1 + \zeta^2\sigma_2 + \cdots. \tag{27}$$

Following the same procedure as done by Maruthi Prasad et al. (2015) the solution for temperature profile and nanoparticle phenomena can be written for $\zeta = 1$ as

$$\theta_t(r,z) = \left(\frac{r^4-h^4}{64}\right)(N_b - N_t), \tag{28}$$

$$\sigma(r,z) = -\left(\frac{r^2-h^2}{4}\right)\frac{N_t}{N_b}. \tag{29}$$

Substituting the Equations (28) and (29) into Equation (14) and applying boundary conditions (18) - (21), the closed form solution for velocity in the core region is obtained as

$$w = \frac{r^2}{4}\frac{dp}{dz} - \frac{G_r}{64}(N_b - N_t)\left(\frac{r^6}{36} - \frac{r^2{h_1}^4}{4}\right) + B_r\left(\frac{N_t}{N_b}\right)\left(\frac{r^4}{16} - \frac{r^2{h_1}^2}{4}\right) + c_4, \tag{30}$$

where

$$c_4 = \frac{dp}{dz}\left(\frac{{h_1}^2-h^2}{4\bar{\mu}} - \frac{{h_1}^2}{4}\right) - \frac{G_r}{288}(N_b - N_t){h_1}^6 + \frac{3B_r}{64}\left(\frac{N_t}{N_b}\right){h_1}^4 + \frac{c_1}{\bar{\mu}}log\left(\frac{h_1}{h}\right),$$

and

$$c_1 = G_r(N_b - N_t)\left(\frac{{h_1}^6}{192}\right) - B_r\left(\frac{N_t}{N_b}\right)\left(\frac{{h_1}^4}{4}\right).$$

The dimensionless flux in the moving frame is given as

$$q = \int_0^{h_1} 2rwdr + \int_{h_1}^{h} 2rw_1 dr. \tag{31}$$

Substituting Equations (22) and (30) into Equation (31), the flux is

$$q = -\frac{dp}{dz}S + G_r(N_b - N_t)\left[\frac{-5{h_1}^8}{192\bar{\mu}} - \frac{h^2{h_1}^6}{768\bar{\mu}} + \frac{{h_1}^8}{768\bar{\mu}} + log\left(\frac{h_1}{h}\right)\left(\frac{{h_1}^8}{192\bar{\mu}} - \frac{h^2{h_1}^6}{388\bar{\mu}}\right)\right] + B_r\left(\frac{N_t}{N_b}\right)\left[\frac{{h_1}^6}{48} + \frac{h^2{h_1}^4}{16\bar{\mu}} - \frac{{h_1}^6}{16\bar{\mu}} - log\left(\frac{h_1}{h}\right)\left(\frac{{h_1}^6}{4\bar{\mu}} + \frac{h^2{h_1}^4}{8\bar{\mu}}\right)\right], \tag{32}$$

where

$$S = \frac{{h_1}^4}{8} + \frac{{h_1}^4}{8\bar{\mu}} + \frac{h^4}{8\bar{\mu}} + \frac{h^2{h_1}^2}{2\bar{\mu}}.$$

The pressure gradient $\frac{dp}{dz}$ is obtained from Equation (32) and is

$$\frac{dp}{dz} = -\frac{q}{S} + \frac{G_r(N_b - N_t)}{S}\left[\frac{-5{h_1}^8}{192\bar{\mu}} - \frac{h^2{h_1}^6}{768\bar{\mu}} + \frac{{h_1}^8}{768\bar{\mu}} + log\left(\frac{h_1}{h}\right)\left(\frac{{h_1}^8}{192\bar{\mu}} - \frac{h^2{h_1}^6}{388\bar{\mu}}\right)\right] + \frac{B_r}{S}\left(\frac{N_t}{N_b}\right)\left[\frac{{h_1}^6}{48} + \frac{h^2{h_1}^4}{16\bar{\mu}} - \frac{{h_1}^6}{16\bar{\mu}} - log\left(\frac{h_1}{h}\right)\left(\frac{{h_1}^6}{4\bar{\mu}} + \frac{h^2{h_1}^4}{8\bar{\mu}}\right)\right]. \tag{33}$$

The pressure drop over the wavelength ΔP_λ is defined as

$$\Delta P_\lambda = -\int_0^1 \frac{dP}{dz} dz. \tag{34}$$

Substituting the expression $\frac{dp}{dz}$ in Equation (34), the pressure drop is

$$\Delta P_\lambda = qL_1 + L_2, \tag{35}$$

where

$$L_1 = \int_0^1 \frac{1}{S}\, dz, \tag{36}$$

$$L_2 = G_r(N_b - N_t)\int_0^1 \left(\frac{\frac{5{h_1}^8}{192\bar{\mu}} + \frac{h^2{h_1}^6}{768\bar{\mu}} - \frac{{h_1}^8}{768\bar{\mu}} - log\left(\frac{h_1}{h}\right)\left(\frac{{h_1}^8}{192\bar{\mu}} - \frac{h^2{h_1}^6}{388\bar{\mu}}\right)}{S}\right)dz - B_r\left(\frac{N_t}{N_b}\right)\int_0^1 \left(\frac{\frac{{h_1}^6}{48} + \frac{h^2{h_1}^4}{16\bar{\mu}} - \frac{{h_1}^6}{16\bar{\mu}} - log\left(\frac{h_1}{h}\right)\left(\frac{{h_1}^6}{4\bar{\mu}} + \frac{h^2{h_1}^4}{8\bar{\mu}}\right)}{S}\right)dz. \tag{37}$$

Following the analysis of Shapiro et al. (1969) the time averaged flux over a period in the laboratory frame $\bar{Q}$ is given as

$$\bar{Q} = 1 + \frac{\epsilon^2}{2} + q. \tag{38}$$

Substituting Equation (38) into Equation (35), the time averaged flux is

$$\bar{Q} = 1 + \frac{\epsilon^2}{2} + \frac{\Delta P_\lambda}{L_1} - \frac{L_2}{L_1}. \tag{39}$$

The dimensionless frictional force $\bar{F}$ at the wall is

$$\bar{F} = \int_0^1 h^2 \left(-\frac{dP}{dz}\right) dz. \tag{40}$$

3.1. Heat Transfer Coefficient

The heat transfer coefficient at the wall is given as

$$Z_\theta(r,z) = \left(\frac{\partial h}{\partial z}\right)\left(\frac{\partial \theta_t}{\partial r}\right). \tag{41}$$

3.2. Mass Transfer Coefficient

The mass transfer coefficient at the wall is given as

$$Z_\sigma(r,z) = \left(\frac{\partial h}{\partial z}\right)\left(\frac{\partial \sigma}{\partial r}\right). \tag{42}$$

4. Results and Discussion

The effects of various parameters on pressure rise, time averaged flux, frictional force, heat transfer coefficient and mass transfer coefficient have been computed numerically and the results are presented graphically using Mathematica 9.0 software.

4.1. Pressure Rise Characteristics

Effects of various parameters like viscosity ratio $(\bar{\mu})$, mean radius of the central layer (δ), Brownian motion parameter (N_b), thermophoresis parameter (N_t), local temperature Grashof number (G_r), local nanoparticle Grashof number (B_r) on pressure rise $(-\Delta p_\lambda)$ are shown in Figures 1.1 - 1.6.

It is observed from Figures 1.1 - 1.6 that, pressure rise $(-\Delta p_\lambda)$ decreases with the increase of time averaged flux $(\bar{Q})$ for fixed values of viscosity ratio $(\bar{\mu})$, mean radius of the central

layer (δ), Brownian motion parameter (N_b), thermophoresis parameter (N_t), local temperature Grashof number (G_r) and local nanoparticle Grashof number (B_r).

It is observed from Figures 1.1, 1.4, 1.5 and 1.6 that, pressure rise $(-\Delta p_\lambda)$ increases with the increase of viscosity ratio $(\bar{\mu})$, thermophoresis parameter (N_t), local temperature Grashof number (G_r) and with local nanoparticle Grashof number (B_r). It is also observed that, when time averaged flux $(\bar{Q})$ reaches 1.0, pressure rise $(-\Delta p_\lambda)$ converges. (From Figure 1.1)

From Figures 1.2 and 1.3, it is noticed that the pressure rise $(-\Delta p_\lambda)$ decreases with the increase of mean radius of the central layer (δ) and with Brownian motion parameter (N_b).

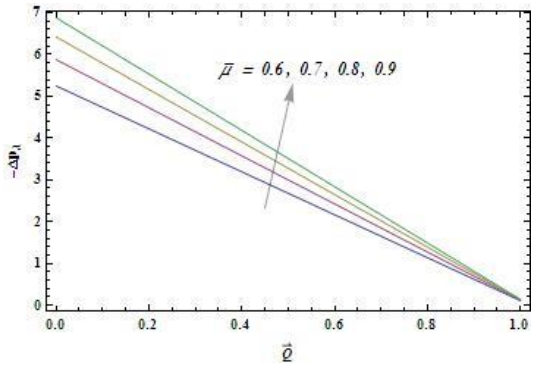

Figure 1.1: Effect of $\bar{Q}$ and $\bar{\mu}$ on $(-\Delta p_\lambda)$
$\left(\epsilon = 0.2, G_r = 0.5, B_r = 0.3, N_b = 1.3, \delta = 0.3, N_t = 1.8\right)$

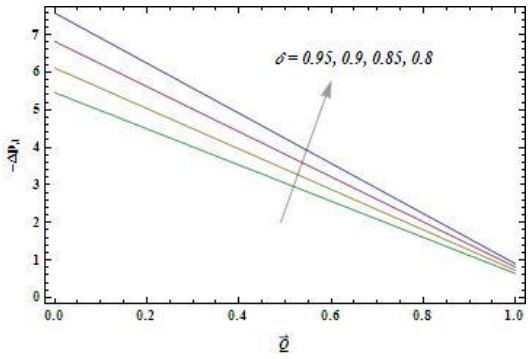

Figure 1.2: Effect of $\bar{Q}$ and δ on $(-\Delta p_\lambda)$
$\left(\epsilon = 0.5, G_r = 0.5, B_r = 0.3, N_b = 1.3, \bar{\mu} = 0.5, N_t = 1.8\right)$

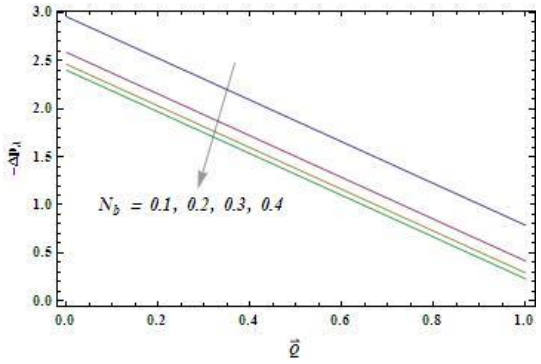

Figure 1.3: Effect of $\bar{Q}$ and N_b on $(-\Delta p_\lambda)$
$\left(\epsilon = 0.2, G_r = 0.5, B_r = 0.3, \delta = 0.8, \bar{\mu} = 0.5, N_t = 1.8\right)$

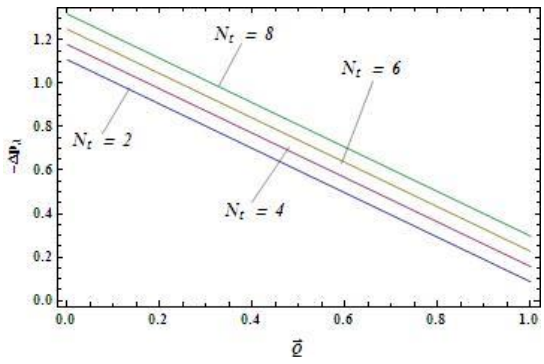

Figure 1.4: Effect of $\bar{Q}$ and N_t on $(-\Delta p_\lambda)$
$\left(\epsilon = 0.2, G_r = 0.5, B_r = 0.3, \delta = 0.9, \bar{\mu} = 0.2, N_b = 1.3\right)$

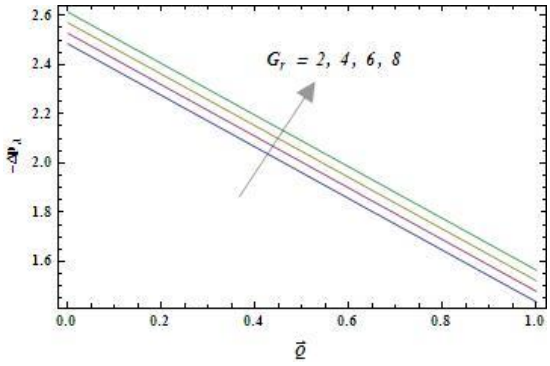

Figure 1.5: Effect of $\bar{Q}$ and G_r on $(-\Delta p_\lambda)$
$\left(\epsilon = 0.5, N_t = 7.8, B_r = 5.3, \delta = 0.8, \bar{\mu} = 0.05, N_b = 7.3\right)$

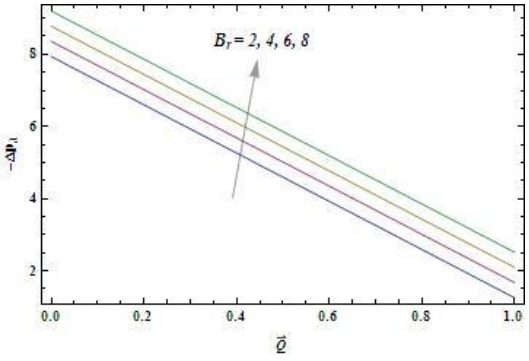

Figure 1.6: Effect of $\bar{Q}$ and B_r on $(-\Delta p_\lambda)$
$\left(\epsilon = 0.5, G_r = 0.5, N_t = 1.8, \delta = 0.8, \bar{\mu} = 0.5, N_b = 1.3\right)$

4.2. Frictional Force

Figures 2.1 - 2.6 show the effect of various parameters on frictional force$(\bar{F})$. It is observed from figures 2.1 - 2.6 that, frictional force decreases with the increase of time averaged flux $(\bar{Q})$ for fixed values of viscosity ratio $(\bar{\mu})$, mean radius of the central layer (δ), Brownian motion parameter (N_b), thermophoresis parameter (N_t), local temperature Grashof number (G_r) and local nanoparticle Grashof number (B_r).

It can be seen from Figures 2.1, 2.4, 2.5 and 2.6 that frictional force $(\bar{F})$ increases with the increase of viscosity ratio $(\bar{\mu})$, thermophoresis parameter (N_t), local temperature Grashof number (G_r) and with local nanoparticle Grashof number (B_r).

From Figures 2.2 and 2.3, it is observed that the frictional force $(\bar{F})$ decreases with the increase of mean radius of the central layer (δ) and with Brownian motion parameter (N_b). It is interesting to observe from Figure 2.2 that, when time averaged flux $(\bar{Q})$ reaches to 1.0, frictional force $(\bar{F})$ converges.

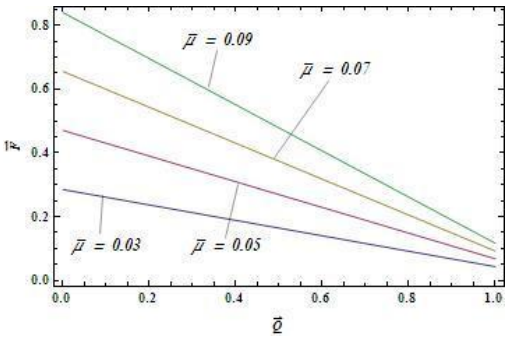

Figure 2.1: Effect of $\bar{Q}$ and $\bar{\mu}$ on $\bar{F}$
$\left(\epsilon = 0.1, G_r = 0.5, B_r = 0.3, N_b = 1.3, \delta = 0.3, N_t = 1.8\right)$

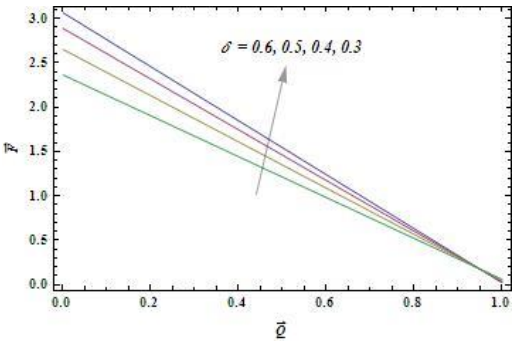

Figure 2.2: Effect of $\bar{Q}$ and δ on $\bar{F}$
$\left(\epsilon = 0.1, G_r = 0.5, B_r = 0.3, N_b = 1.3, \bar{\mu} = 0.4, N_t = 1.8\right)$

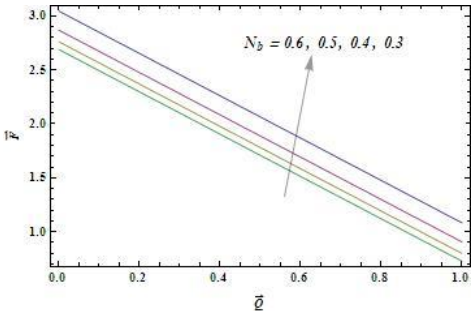

Figure 2.3: Effect of $\overline{Q}$ and N_b on $\overline{F}$
$\left(\epsilon = 0.6, G_r = 0.5, B_r = 0.3, \delta = 0.8, \overline{\mu} = 0.2, N_t = 1.8\right)$

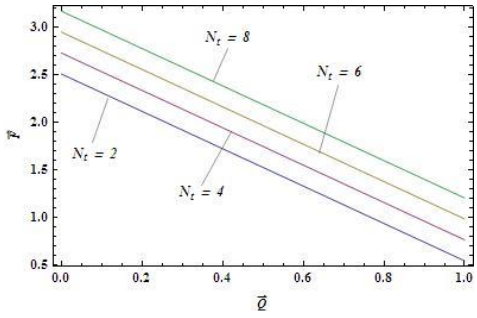

Figure 2.4: Effect of $\overline{Q}$ and N_t on$\overline{F}$
$\left(\epsilon = 0.6, G_r = 0.5, B_r = 0.3, \delta = 0.8, \overline{\mu} = 0.2, N_b = 1.3\right)$

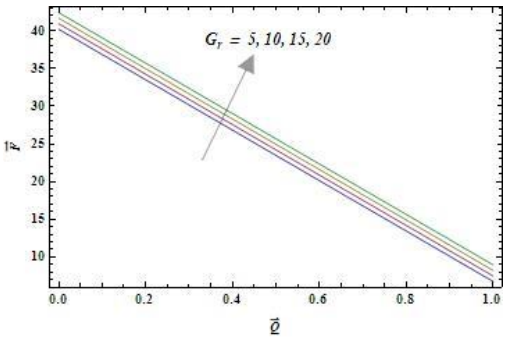

Figure 2.5: Effect of $\overline{Q}$ and G_r on$\overline{F}$
$\left(\epsilon = 0.5, N_t = 1.8, B_r = 0.3, \delta = 0.99, \overline{\mu} = 0.05, N_b = 1.3\right)$

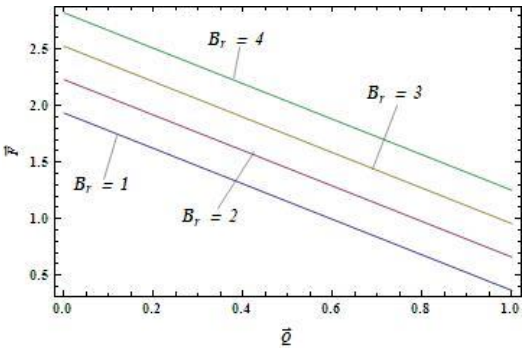

Figure 2.6: Effect of $\overline{Q}$ and B_r on$\overline{F}$
$\left(\epsilon = 0.3, G_r = 0.5, N_t = 1.8, \delta = 0.8, \overline{\mu} = 0.3, N_b = 1.3\right)$

4.3. Temperature Profile

Effects of Brownian motion parameter (N_b) and thermophoresis parameter (N_t) on temperature profile (θ_t) have been shown in Figures 3.1-3.2. It is noticed from Figure 3.1 that, with the increase of Brownian motion parameter (N_b), temperature profile (θ_t) increases in the region $r \in [-1, -0.8]$ and in the region $r \in [0.8,\ 1]$, but decreases in the region $r \in [-0.8,\ 0.8]$. However, temperature profile (θ_t) shows an opposite behaviour with thermophoresis parameter (N_t).

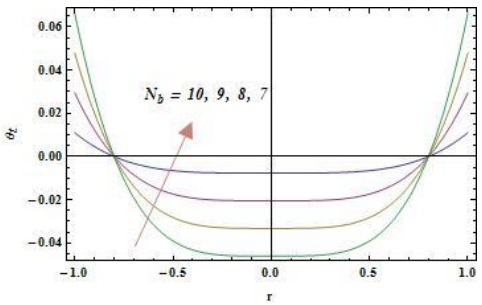

Figure 3.1: Variation in Temperature profile with N_b
$(Z = 1.5, \epsilon = 0.9, N_t = 1.8, \delta = 0.8)$

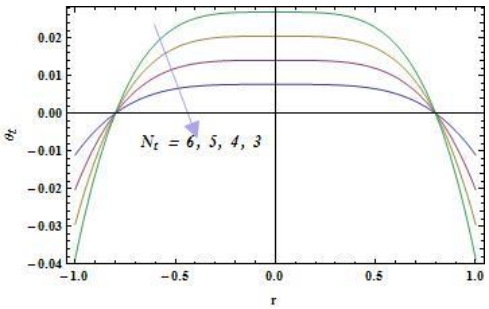

Figure 3.2: Variation in Temperature profile with N_t
$(Z = 3, \epsilon = 0.9, N_b = 0.1, \delta = 0.8)$

4.4. Nanoparticle Phenomena

The nature of nanoparticle phenomena (σ) for different values of Brownian motion parameter (N_b) and thermophoresis parameter (N_t) can be observed from Figures 4.1 - 4.2. It is observed that, nanoparticle phenomena (σ) decreases with the increase of Brownian motion parameter (N_b) in the regions $r \in [-1, -0.8]$, $r \in [0.8,\ 1]$ and increases in the region $r \in [-0.8,\ 0.8]$. It is interesting to observe that nanoparticle phenomena (σ) reaches maximum at $r = 0$. However, it shows an opposite behaviour with thermophoresis parameter (N_t).

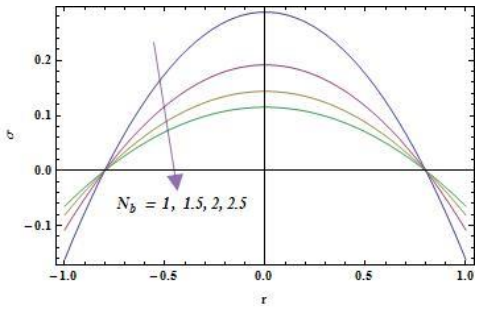

Figure 4.1: Variation in Nanoparticle Phenomenon with N_b
$(Z = 1, \epsilon = 0.5, N_t = 1.8, \delta = 0.8)$

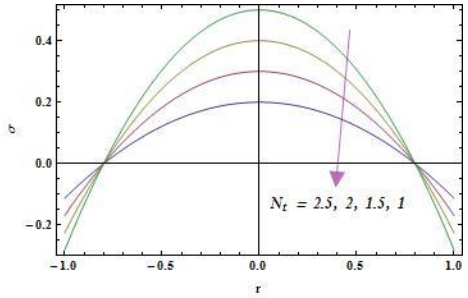

Figure 4.2: Variation in Nanoparticle Phenomenon with N_t
$(Z = 1, \epsilon = 0.9, N_b = 1.8, \delta = 0.8)$

4.4. Heat Transfer Coefficient

Figures 5.1 - 5.3 explain the variation of heat transfer coefficient (Z_θ) for various values of Brownian motion parameter (N_b), thermophoresis parameter (N_t) and amplitude ratio (ϵ). From Figures 5.2 and 5.3, it is observed that the value of the heat transfer coefficient (Z_θ) increases with thermophoresis parameter $(N_t)$and amplitude ratio (ϵ) and then decreases after attaining a constant value. However, heat transfer coefficient (Z_θ) shows an opposite behaviour with respect to Brownian motion parameter (N_b) (from Figure 5.1). It is interesting to observe that there is no significant change in the heat transfer coefficient (Z_θ) value in the region $r\epsilon[-0.2, 0.2]$.

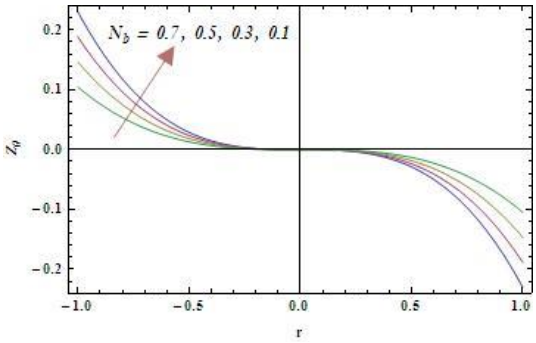

Figure 5.1: Variation in heat transfer coefficient with N_b
$(Z = 4, \epsilon = 0.2, N_t = 1.2, \delta = 0.8)$

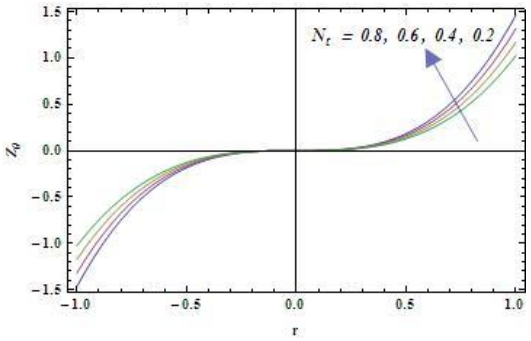

Figure 5.2: Variation in heat transfer coefficient with N_t
$(Z = 3, \epsilon = 0.7, N_b = 2.2, \delta = 0.8)$

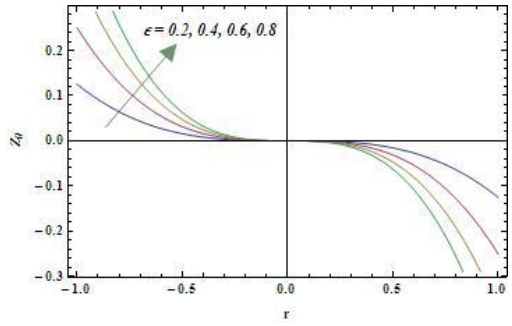

Figure 5.3: Variation in heat transfer coefficient with ϵ
($Z = 4.2, N_t = 0.8, N_b = 0.2, \delta = 0.8$)

4.5. Mass Transfer Coefficient

Figures 6.1 - 6.3 indicate the effect of various parameters on mass transfer coefficient(Z_σ). It is noticed that mass transfer coefficient (Z_σ) decreases with the increase of Brownian motion parameter (N_b), thermophoresis parameter(N_t) and then increases after attaining a constant value $r = 0$. However, mass transfer coefficient(Z_σ) shows an opposite behaviour with respect to amplitude ratio(ϵ). It is interesting to observe that mass transfer coefficient (Z_σ) converges in the region $r\epsilon[-1, 0]$ and diverges in the region $r\epsilon[0, 1]$.

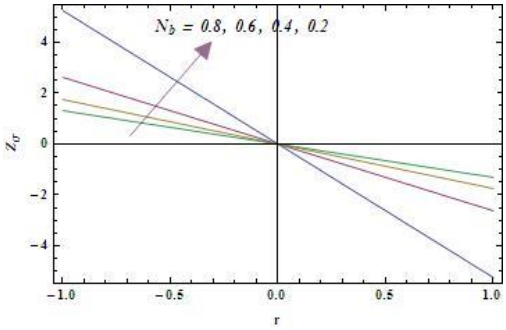

Figure 6.1: Variation in Mass transfer coefficient with N_b
($Z = 3.2, \epsilon = 0.9, N_t = 1.2, \delta = 0.8$)

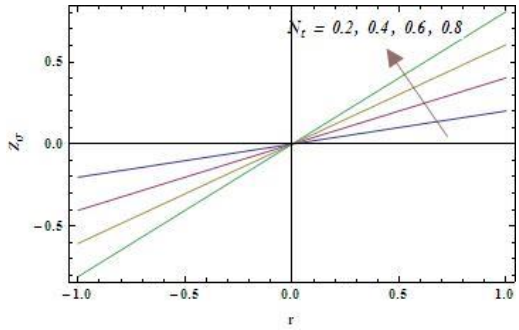

Figure 6.2: Variation in Mass transfer coefficient with N_t
($Z = 1.5, \epsilon = 0.9, N_b = 2.8, \delta = 0.8$)

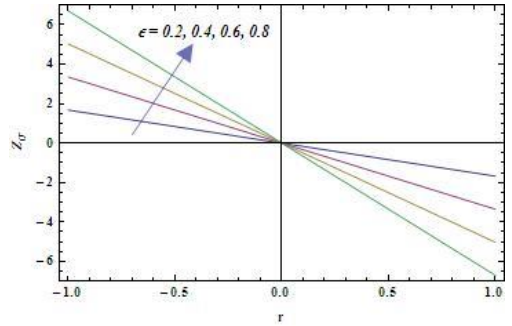

Figure 6.3: Variation in Mass transfer coefficient with ϵ
($Z = 3, N_t = 0.8, N_b = 0.3, \delta = 0.8$)

4.6. Velocity Profiles

The variation in velocity profiles in the core region can be observed from Figures 7.1 - 7.5. It is observed that velocity profiles increase in the radial direction for fixed values of velocity ratio $(\bar{\mu})$, thermophoresis parameter (N_t), local temperature Grashof number (G_r) and local nanoparticle Grashof number (B_r).

It is also observed that velocity profiles decrease with the increase of velocity ratio $(\bar{\mu})$, mean radius of the central layer (δ), thermophoresis parameter (N_t), local temperature Grashof number (G_r) and local nanoparticle Grashof number (B_r).

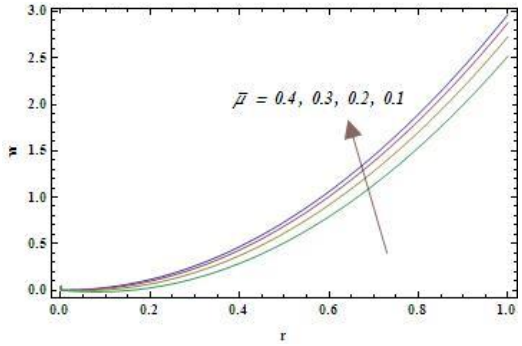

Figure 7.1: Variation in velocity profile w with $\bar{\mu}$
$(\epsilon = 0.5, G_r = 0.05, B_r = 0.03, N_b = 0.03, \delta = 0.01, N_t = 0.08, \bar{Q} = 1.5, z = 0.5)$

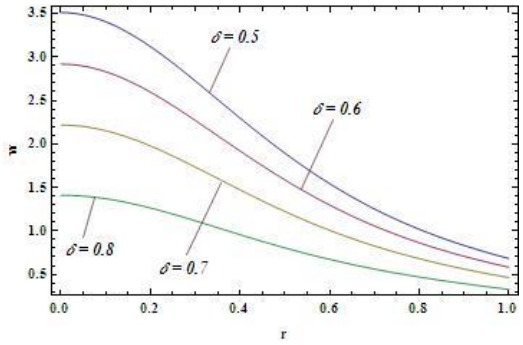

Figure 7.2: Variation in velocity profile w with δ
$(\epsilon = 0.9, G_r = 0.5, B_r = 0.3, N_b = 0.3, \bar{\mu} = 0.9, N_t = 0.8, \bar{Q} = 3, z = 2.5)$

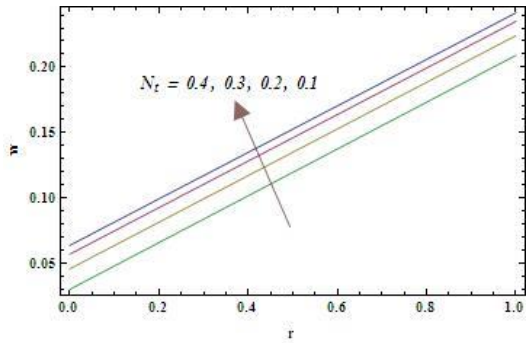

Figure 7.3: Variation in velocity profile w with N_t
$(\epsilon = 0.2, G_r = 0.5, B_r = 0.3, \delta = 0.5, \bar{\mu} = 0.06, N_b = 0.3, \bar{Q} = 2, z = 2)$

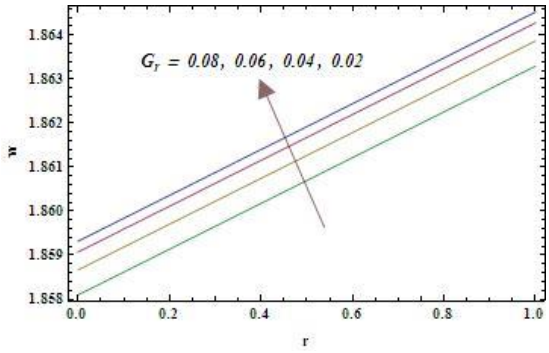

Figure 7.4: Variation in velocity profile w with G_r
$(\epsilon = 0.5, N_t = 1.8, B_r = 1.3, \delta = 0.8, \bar{\mu} = 0.1, N_b = 0.3, \bar{Q} = 2, z = 3)$

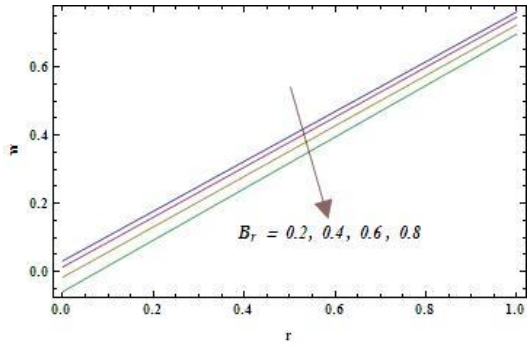

Figure 7.5: Variation in velocity profile w with B_r
$(\epsilon = 0.2, N_t = 0.8, G_r = 0.3, \delta = 0.5, \bar{\mu} = 0.04, N_b = 0.3, \bar{Q} = 2, z = 3)$

4.7. Streamline Patterns

The formulation of an internally circulating bolus of the fluid by closed streamline is called trapping. This trapped bolus is pulled ahead along with the peristaltic wave. Figures 8.1-8.7 explain the streamline patterns and trapping for different values of viscosity ratio, mean radius of the central layer, Brownian motion parameter, thermophoresis parameter, local temperature Grashof number, local nanoparticle Grashof number and amplitude ratio.

From Figures 8.1, 8.2, 8.3 and 8.7, it is noticed that the volume of trapped bolus decreases with the increase of viscosity ratio, mean radius of the central layer, Brownian motion parameter (N_b) and with amplitude ratio (ϵ).

From Figures 8.4, 8.5 and 8.6, it is observed that, the volume of the trapped bolus increases with the increase of thermophoresis parameter (N_t), local temperature Grashof number (G_r) and with the local nanoparticle Grashof number (B_r).

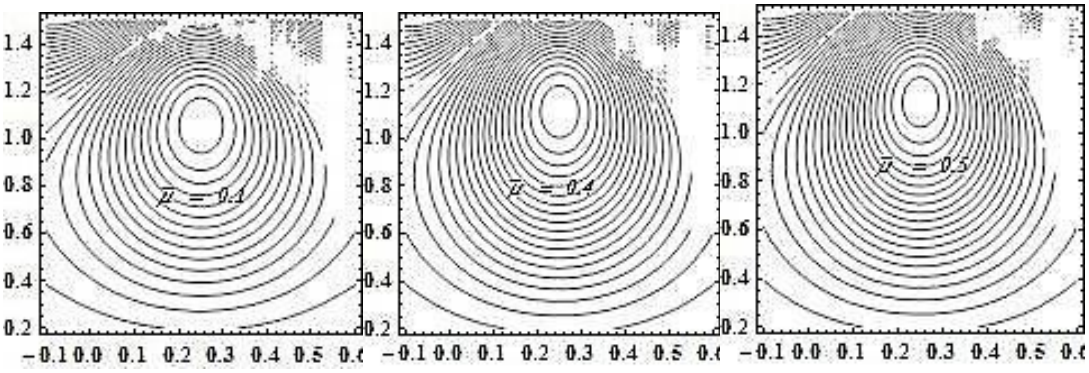

Figure 8.1: Stream line patterns for different values of $\bar{\mu}$
$(\epsilon = 0.2, \bar{Q} = 0.7, G_r = 5, B_r = 3, N_b = 7, N_t = 3, \delta = 0.9)$

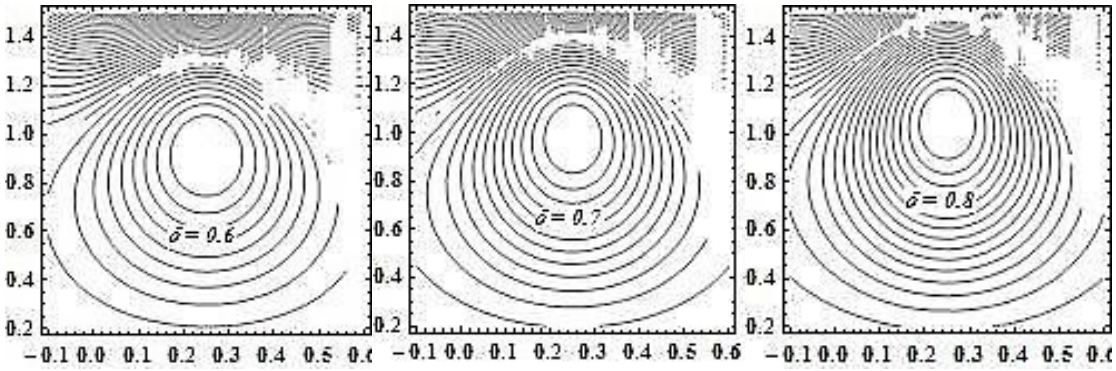

Figure 8.2: Stream line patterns for different values of δ
$(\epsilon = 0.2, \bar{Q} = 0.7, G_r = 5, B_r = 3, N_b = 7, N_t = 3, \bar{\mu} = 0.4)$

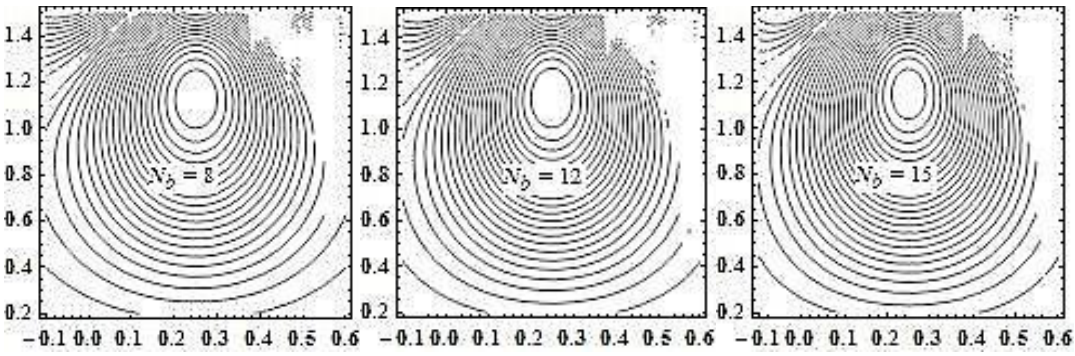

Figure 8.3: Stream line patterns for different values of N_b
$(\epsilon = 0.2, \bar{Q} = 0.7, G_r = 5, B_r = 3, \delta = 0.9, N_t = 3, \bar{\mu} = 0.5)$

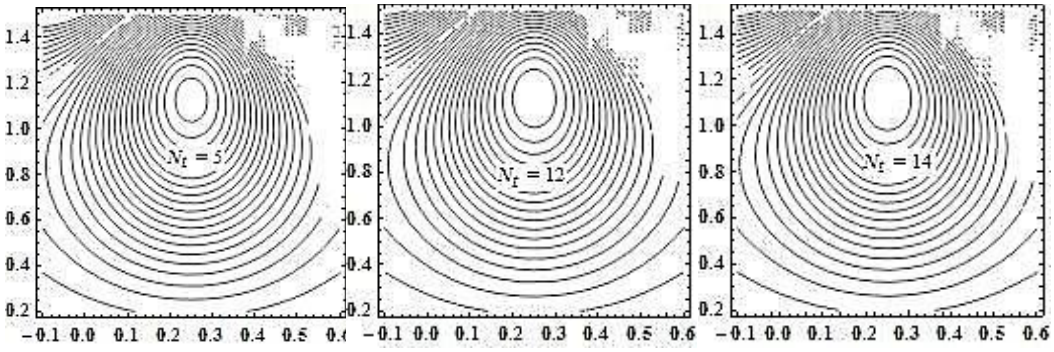

Figure 8.4: Stream line patterns for different values of N_t
$(\epsilon = 0.2, \bar{Q} = 0.7, G_r = 5, B_r = 3, \delta = 0.9, N_b = 7, \bar{\mu} = 0.5)$

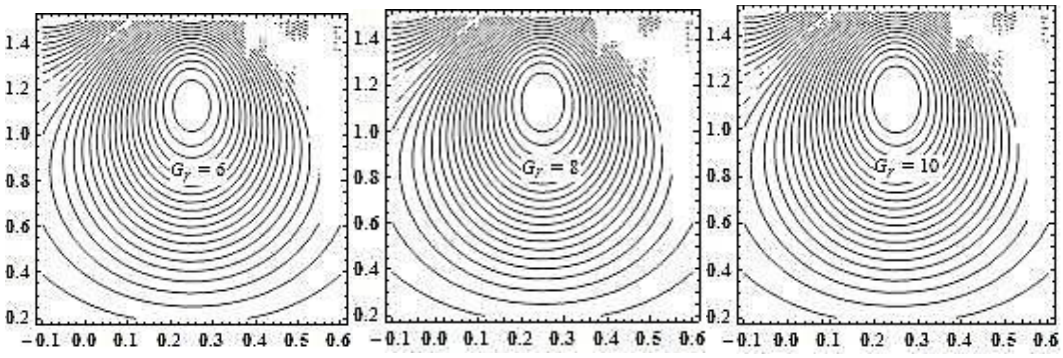

Figure 8.5: Stream line patterns for different values of G_r
$(\epsilon = 0.2, \bar{Q} = 0.7, N_t = 3, B_r = 3, \delta = 0.9, N_b = 7, \bar{\mu} = 0.5)$

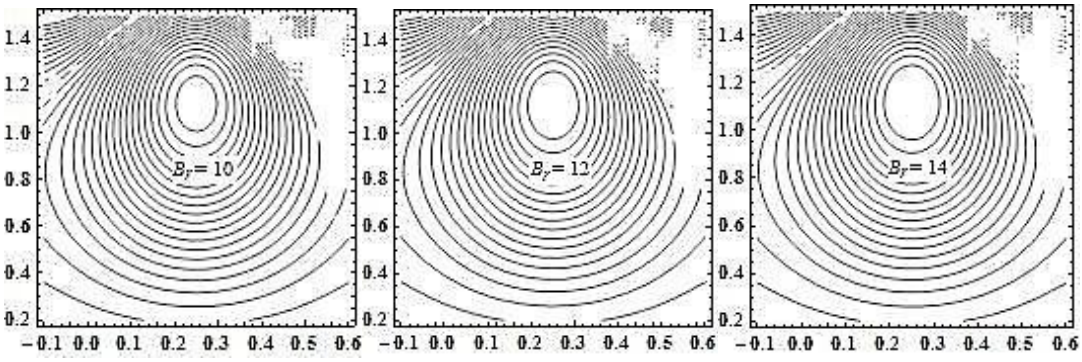

Figure 8.6: Stream line patterns for different values of B_r
$(\epsilon = 0.2, \bar{Q} = 0.7, N_t = 3, G_r = 5, \delta = 0.9, N_b = 7, \bar{\mu} = 0.5)$

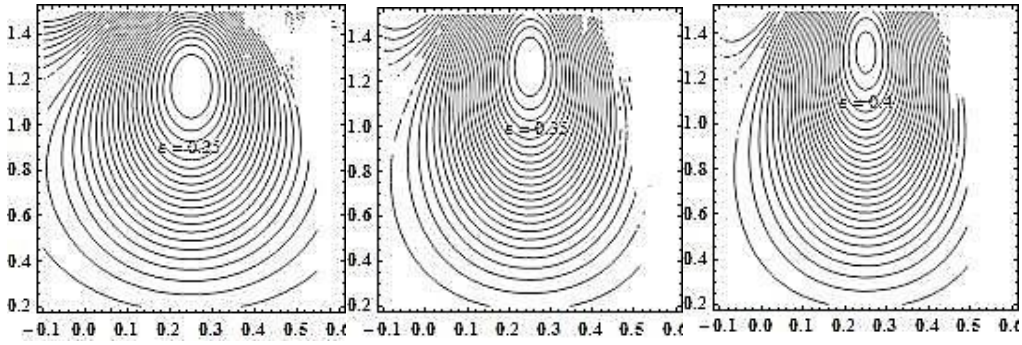

Figure 8.7: Stream line patterns for different values of ϵ
$(B_r = 5, \bar{Q} = 0.7, N_t = 3, G_r = 5, \delta = 0.9, N_b = 7, \bar{\mu} = 0.5)$

5. Conclusion

The present study deals with heat and mass transfer effects of peristaltic transport of a nanofluid in peripheral layer under the approximations of low Reynold's number and long wave length. Emphasis has been laid on investigating pressure drop, frictional force, temperature profile in the

core region as well as peripheral region, nanoparticle phenomenon, heat transfer coefficient, mass transfer coefficient, velocity profiles and streamline patterns for the nano fluid for the variables like viscosity ratio, mean radius of the central layer, Brownian motion parameter, thermophoresis parameter, local temperature Grashof number and local nanoparticle Grashof number. Homotopy perturbation method has been used to solve the nonlinear coupled equations of temperature profile and nanoparticle phenomena.

The main points of the analysis are as follows:

a. The pressure rise increases with the increase of viscosity ratio, thermophoresis parameter, local temperature Grashof number, local nanoparticle Grashof number and decreases with the increase of mean radius of the central layer and Brownian motion parameter.

b. The frictional force increases with the increase of viscosity ratio, thermophoresis parameter, local temperature Grashof number, local nanoparticle Grashof number and decreases with the increase of mean radius of the central layer and Brownian motion parameter.

c. With the increase of Brownian motion parameter, temperature profile increases in the region $r \in [-1, -0.8]$ and in the region $r \in [0.8,\ 1]$, but decreases in the region $r \in [-0.8,\ 0.8]$. However, temperature profile shows opposite behaviour with thermophoresis parameter.

d. Nanoparticle phenomenon decreases with the increase of Brownian motion parameter in the regions $r \in [-1, -0.8]$, $r \in [0.8,\ 1]$ and increases in the region $r \in [-0.8,\ 0.8]$. Nanoparticle phenomena reach maximum at $r = 0$. However, it shows an opposite behaviour with thermophoresis parameter.

e. Heat transfer coefficient increases with the increase of thermophoresis parameter and amplitude ratio; and shows an opposite behaviour with the increase of Brownian motion parameter.

f. Mass transfer coefficient converges in the region $r\epsilon[-1, 0]$ and diverges in the region $r\epsilon[0, 1]$ with the increase of Brownian motion parameter and thermophoresis parameter and amplitude ratio.

g. Velocity profiles in the core region increase in the radial direction for fixed values of velocity ratio, thermophoresis parameter, local temperature Grashof number and local nanoparticle Grashof number.

h. Velocity profiles decrease with the increase of velocity ratio, mean radius of the central layer, thermophoresis parameter, local temperature Grashof number and local nanoparticle Grashof number.

i. The volume of the trapped bolus increases with the increase of thermophoresis parameter, local temperature Grashof number, local nanoparticle Grashof number and decreases with

the increase of viscosity ratio, mean radius of the central layer, Brownian motion parameter and amplitude ratio.

REFERENCES

Brasseur, J. G. Corrsin, S., and Lu, N. Q. (1987). The influence of a peripheral layer of different viscosity on peristaltic pumping with Newtonian fluids. *Journal of Fluid Mechanics*, *174*, 495–519.

Devi, R. G. and Devanathan, R. (1975). Peristaltic motion of a micropolar fluid (Vol. 81, pp. 149–163). Presented at the Proceedings of the Indian Academy of Sciences-Section A, Springer.

Fung, Y. C. and Yih, C. S. (1968). Peristaltic Transport. *Journal of Applied Mechanics*, *35*(4), 669–675.

He, J.-H. (1998). Approximate analytical solution for seepage flow with fractional derivatives in porous media. *Computer Methods in Applied Mechanics and Engineering, Volume 167, Issues 1-2, 1 December 1998, Pages 57-68.*

Latham, T. W. (1966). *Fluid motions in a peristaltic pump.* (Thesis). Massachusetts Institute of Technology.

Li, M. and Brasseur, J. G. (1993). Non-steady peristaltic transport in finite-length tubes. *Journal of Fluid Mechanics*, *248*, 129–151.

Nadeem, S., Riaz, A., Ellahi, R. and Akbar, N. (2014). Effects of heat and mass transfer on peristaltic flow of a nanofluid between eccentric cylinders. *Applied Nanoscience*, *4*(4), 393–404.

Noreen Sher Akbar, S. N. (2012). Erratum to: Peristaltic flow of a nanofluid in a non-uniform tube. *Heat and Mass Transfer*, *48*(3), 451–459.

Pincombe, B., Mazumdar, J. and Hamilton-Craig, I. (1999). Effects of multiple stenoses and post-stenotic dilatation on non-Newtonian blood flow in small arteries. *Medical & Biological Engineering & Computing*, *37*(5), 595–599.

Prasad K., M., N., S. and M.A.S., S. (2015). Study of Peristaltic Motion of Nano Particles of a Micropolar Fluid with Heat and Mass Transfer Effect in an Inclined Tube. *INTERNATIONAL CONFERENCE ON COMPUTATIONAL HEAT AND MASS TRANSFER (ICCHMT) - 2015*, *127*, 694–702.

Prasad, K. M. and Radhakrishnamacharya, G. (2009). Effect of Peripheral Layer on Peristaltic Transport of a Couple Stress Fluid. *International Journal of Fluid Mechanics Research*, *36*(6).

Prasad, K. M., Subadra, N. and Srinivas, M. (2015). Peristaltic Transport of a Nanofluid in an Inclined Tube. *American Journal of Computational and Applied Mathematics*, *5*(4), 117–128.

Prasad, K. and Radhakrishnamacharya, G. (2009). Effect of peripheral layer on peristaltic transport of a micropolar fluid.

Rao, A. R. and Usha, S. (1995). Peristaltic transport of two immiscible viscous fluids in a circular tube. *Journal of Fluid Mechanics*, *298*, 271–285.

Santhosh, N., Radhakrishnamacharya, G. and Chamkha, A. J. (2015). FLOW OF A JEFFREY FLUID THROUGH A POROUS MEDIUM IN NARROW TUBES. *Journal of Porous Media*, *18*(1), 71–78.

Shapiro, A. H., Jaffrin, M. Y. and Weinberg, S. L. (1969). Peristaltic pumping with long wavelengths at low Reynolds number. *Journal of Fluid Mechanics*, *37*(04), 799–825.

Shukla, J. B., Parihar, R. S., Rao, B. R. P., & Gupta, S. P. (1980). Effects of peripheral-layer viscosity on peristaltic transport of a bio-fluid. *Journal of Fluid Mechanics*, *97*(02), 225–237.

Srivastava, L. M., & Srivastava, V. P. (1982). Peristaltic transport of a two-layered model of physiological fluid. *Journal of Biomechanics*, *15*(4), 257–265.

S. U.S. Choi, J. A. E. (1995). Enhancing thermal conductivity of fluids with nanoparticles. ASME FED. *Proceedings of the ASME International Mechanical Engineering Congress and Exposition*, *66*.